Promoting Bioengineered Tooth Innervation Using Nanostructured and Hybrid Scaffolds

S. Kuchler-Bopp[a,b]*, A. Larrea[c,d], L. Petry[a,b], Y. Idoux-Gillet[a,b], V. Sebastian[c,d], A. Ferrandon[a,b], P. Schwinté[a,b], M. Arruebo[c,d], N. Benkirane-Jessel[a,b]

[a]*INSERM, UMR 1109, Osteoarticular and Dental Regenerative NanoMedicine Laboratory: http://www.regmed.fr, FMTS, 11 rue Humann, Strasbourg, Strasbourg.*

[b]*Université de Strasbourg, Faculté de Chirurgie Dentaire, 1 place de l'Hôpital, Strasbourg F-67000, France.*

[c]*CIBER de Bioingeniería, Biomateriales y Nanomedicina (CIBER-BBN), Centro de Investigación Biomédica en Red. C/ Monforte de Lemos 3-5, Pabellón 11, 28029 Madrid.*

[d]*Department of Chemical and Environmental Engineering and Aragon Nanoscience Institute, University of Zaragoza, C/Mariano Esquillor, s/n, Zaragoza 50018, Spain.*

*corresponding author: INSERM UMR 1109, 11 rue Humann, 67000 Strasbourg, France, phone number: (33)-3-68-85-33-76, fax number: (33)-3-68-85-33-01, Email address: kuchler@unistra.fr

Abbreviated title: CsA-loaded PLGA scaffold for innervation

Abstract

The innervation of teeth mediated by axons originating from the trigeminal ganglia is essential for their function and protection. Immunosuppressive therapy using Cyclosporine A (CsA) was found to accelerate the innervation of transplanted tissues and particularly that of bioengineered teeth. To avoid the CsA side effects, we report in this study the preparation of CsA loaded poly(lactic-co-glycolic acid) (PLGA) nanoparticles, their embedding on polycaprolactone (PCL)-based scaffolds and their possible use as templates for the innervation of bioengineered teeth. This PCL scaffold, approved by the FDA and capable of mimicking the extracellular matrix, was obtained by electrospinning and decorated with CsA-loaded PLGA nanoparticles to allow a local sustained action of this immunosuppressive drug. Dental re-associations were co-implanted with a trigeminal ganglion on functionalized scaffolds containing PLGA and PLGA/Cyclosporine in adult ICR mice during 2 weeks. Histological analyses showed that the designed scaffolds did not alter the teeth development after in vivo implantation. The study of the innervation of the dental re-associations by indirect immunofluorescence and transmission electron microscopy (TEM), showed that 88.4 % of the regenerated teeth were innervated when using the CsA-loaded PLGA scaffold. The development of active implants thus allows their potential use in the context of dental engineering.

Statement of significance

Tooth innervation is essential for their function and protection and this can be promoted in vivo using polymeric scaffolds functionalized with immunosuppressive drug-loaded

nanoparticles. Immunosuppressive therapy using biodegradable nanoparticles loaded with Cyclosporine A was found to accelerate the innervation of bioengineered teeth after two weeks of implantation.

Keywords
Bioengineered tooth; Cyclosporine A; Electrospun polycaprolactone; Innervation; Nanoparticles

1. Introduction

Dental caries, periodontal diseases and oropharyngeal cancers are the most prevalent oral diseases. Dental caries and tooth loss are important oral health indicators for adults and are key measures for monitoring progress of the disease [1]. The National Health and Nutrition Examination Survey, 2011–2012, revealed that in adults aged 20–64, 91% had dental caries and 27% had untreated tooth decay. Only 48% of adults aged 20–64 had a full set of permanent teeth (excluding third molars) and nearly 19% of adults aged 65 and over were edentulous [1]. Current dentures and implants used to replace missing teeth do not remodel and show a reduced integration with the host. Therefore, there is a need for new biomaterials to promote regeneration.

Regenerative nanomedicine is a rapidly expanding domain which has as objective the development of compatible biomaterials accepted by the body able to interact with cells/tissues present in the site of implantation. Such biomaterials can be combined with nanoparticles allowing a controlled or sustained release of active molecules. On the other hand, tissue engineering aims at replacing or repairing damaged tissues.

Keller et al. [2] showed that cultured re-associations between dissociated mesenchymal cells and intact epithelium from Embryonic Day (ED) 14 mouse molars gave well formed teeth after implantation under the skin of adult ICR mice. The vascularization of the dental pulp occurred while the innervation was never observed [2]. Siemionow et al. [3] showed that, immunosuppressive therapy with tacrolimus, a calcineurin inhibitor, accelerated nerve regeneration in the case of face transplantation. Cyclosporine A (CsA), another calcineurin inhibitor, widely used in organ transplantation [4] has also direct effect on nerve growth [5,6]. When cultured re-associations were co-implanted with trigeminal ganglia in CsA-treated ICR mice, the innervation of the dental mesenchyme occurred after one week of implantation. After two weeks, the axons coming from the trigeminal ganglia reached the odontoblasts. These results demonstrated that the innervation of the dental pulp can be obtained in immunosuppressive conditions [7]. However, the oral availability of CsA is slow and highly variable owing to its biopharmaceutical properties. The use of this molecule is controversial because it can induce different forms of kidney dysfunction, cancers and lymphomas [8,9]. Different approaches have been investigated to reduce its nephrotoxicity by developing CsA-loaded PLGA nanoparticles as delivery vehicles because of their excellent biocompatibility and sustained release [10].

On the other hand, the development of compatible biomaterials is also an essential step in the regeneration of a functional tooth as we previously showed by using a FDA approved nanofibrous polycaprolactone (PCL) scaffold functionalized with nerve growth factor (NGF) for a local release of this neurotrophic factor [11]. Indeed, when the scaffold was functionalized with nanoparticles containing NGF the innervation occurred in the dental pulp indicating the capability of the NGF

nanoreservoirs to direct axon formation from the trigeminal ganglion into the bioengineered tooth [11]. So, following this strategy it should be possible to fabricate a combination cell-therapy implant capable of regeneration of a vascularized and innervated tooth as tooth replacement during regenerative therapy.

The aim of this study was to combine a local sustained effect of CsA with the use of a PCL-based scaffold, using reduced doses of the immunosuppressant molecule and so avoiding the unwanted side effects attributed to the ingestion or burst release of this drug. For this purpose, we functionalized PCL scaffolds with CsA-loaded nanoparticles and studied the innervation in the bioengineered teeth pulp by immunofluorescence and transmission electron microscopy (TEM).

2. Materials and Methods

2.1. Materials

Poly (D, L-lactic acid/glycolic acid) 50/50 polymer (PLGA; MW 24-38 KDa), under the commercial name Resomer® RG 503 was purchased from Evonik Industries AG (Darmstadt, Germany). Polycaprolactone (PCL; MW 80 KDa) analytical grade, Cyclosporine A, Dexamethasone (used as HPLC internal standard), Pluronic® F-68 surfactant, ethyl acetate (Class 3 solvent according to the pharmacopeia), acetonitrile and methanol (HPLC grade), were all purchased from Sigma Aldrich (St. Louis (MO), USA) and used as received. All references to water imply the use of MilliQ water previously filtered through a 0.2µm cellulose nitrate membrane.

2.2. Synthesis of Cyclosporine A (CsA) loaded PLGA nanoparticles

Cyclosporine loaded PLGA (PLGA/CsA) nanoparticles were prepared in a continuous microfluidic reactor using a PEEK-made interdigital micromixer (SIMM-V2, Slit Interdigital Micro Mixer, IMM, Mainz, Germany) by carrying out an oil-in-water (O/W) emulsification process followed by a solvent evaporation procedure. Briefly, 1% (w/v) of PLGA (50:50) polymer, 0.1% (w/v) of CsA and 2% (w/v) of Pluronic F68 (used as surfactant) were dissolved in 30 mL of ethyl acetate (used as organic solvent). This resulting organic phase was then mixed and emulsified with MilliQ water, interfaced using syringe pumps (Harvard Apparatus), with flow rates of 16 and 32 mL min^{-1}, respectively. Both solutions were fed through a 1/16" PTFE tubing and then interfaced inside the PEEK-based interdigital micromixer. The micromixer was placed in an ice bath to control the reaction temperature. After the formation of a stable emulsion, the organic solvent was evaporated under continuous stirring (600 rpm) in an open flask during 3 h (Fig. 1).

2.3. Characterization techniques

Scanning electron microscopy (SEM, Inspect F50, FEI, Eindhoven, The Netherlands) was employed to determine the shape of the synthesized PLGA NPs. The freshly prepared nanoparticles were mixed during 1.5 h with the same volume of phosphotungstic acid solution (7.5% w/v) used as contrast agent. The dispersion was then centrifuged and washed three times with Milli Q water and later re-suspended. A drop of the resulting nanoparticle suspension was placed on a glass slide, air dried and coated with platinum under vacuum before SEM observation. Nanoparticle size, size distribution and zeta potential (pH 7.2) were determined by dynamic light scattering (Zeta Plus, Brookhaven Instruments Corporation, NY) after appropriate dilution with Milli Q water. At least five replicate measurements were recorded in each case. CsA

content in PLGA nanoparticles was determined directly by dissolving the drug loaded nanoparticles in a solvent composed of acetonitrile and dexamethasone as HPLC internal standard. Then, methanol was added and the mixture was placed in a sonifier bath for 15 min to promote PLGA precipitation. The resulting dispersion was centrifuged at 12000 rpm for 20 min to remove the polymeric residue and the supernatant was filter using 0.22 μm PTFE syringe filters and placed in a vial for HPLC analysis. Experiments were performed in triplicate. CsA content in the samples was then determined by HPLC (Waters Instrument 2690 Alliance, USA). A Kinetex C18 column with a 2.6 μm particle size filler and column dimensions of 50 mm × 4.6 mm was used. The mobile phase consisted in a 80:20 (v/v) mixture of acetonitrile:water including a phosphoric acid concentration of 200 ppm. The detector wavelength, injection volume, flow rate, and column temperature were 210 nm, 5 μL, 0.5 mL min^{-1} and 70 °C, respectively. The HPLC method was validated with respect to linearity, repeatability and the limit of quantification and limit of detection. Drug encapsulation efficiency (EE) and drug loading (DL) were calculated using the following equations:

Equation (1) $$EE\ (\%) = \frac{\text{Amount of drug loaded}}{\text{Total amount of drug used}} \text{ x } 100$$

Equation (2) $$D\ L\ (\%) = \frac{\text{Amount of drug loaded}}{\text{Amount of PLGA}} \text{ x } 100$$

In vitro drug release studies were carried out using a mini dialysis cassette composed of a 20000 molecular weight cut-off cellulose dialysis membrane (Slide-A-Lyzer, Fischer). The CsA-PLGA nanoparticles in suspension (2 ml with a concentration of 9 mg/ml) were loaded into the dialysis cassette which was immersed in a conical tube with 44 mL of PBS containing 1% (w/v) of tween 80. The tubes were placed in an incubator thermostatted at 37ºC under oscillation at 100 rpm. At predetermined intervals, samples

of the CsA-PLGA were collected and washed by centrifugation. Finally, the entrapment efficiency protocol described above was used to open the nanoparticles and directly determine the drug concentration remaining in the sample at each time point using HPLC.

2.4. PCL scaffold synthesis and functionalization

PCL was dissolved in a mixture of dichloromethane/dimethylformamide (DCM/DMF 50/50 v/v) at 15% wt/v and stirred overnight before use. A standard electrospinning set-up (EC-DIG apparatus, IME Technologies, Eindhoven, Netherlands) was used to fabricate the PCL scaffolds. The PCL solution was poured into a 5 mL syringe and ejected through a needle with a diameter of 0.5 mm at a flow rate of 1.2 mL h^{-1}, with a programmable pump (Harvard apparatus). A high-voltage power supply (SPELLMAN, SL30P10) was used to set 15 kV at the needle. Aluminum foils (20x20 cm^2), connected to the ground collector at a distance of 17 cm from the needle, were used to collect the electrospun PCL scaffold. PCL scaffolds dried in vacuum oven overnight to remove traces of solvent and then functionalized by the layer-by-layer method. All rinse solution used was Tris buffer 20mM/NaCl 0.15 M at pH 7.4. PCL scaffolds were incubated in a poly-L-lysine solution (PLL, 500mg/mL) for 15 min, rinsed with the buffer for 15 min, and then incubated in PLGA or PLGA/CsA nanoparticles solution for 15 min and finally thoroughly washed for 15 min, thus constructing a “bilayer” (PLL/PLGA/CsA) on the fiber surface. Repeating this protocol five times allowed the construction of $(PLL/PLGA/CsA)_5$, respectively. Even though this buffer solution provides with high ionic strength to the media, the nanoparticles remained strongly bound to the PLL electrospun nanofibers as it can be seen in figures 2f and g.

185 2.5. Molar ED14 culture, implant preparation and in vivo implantation

186 The first lower molars were dissected from ICR mouse (Charles River
187 Laboratories, l'Arbresle, France) embryos at Embryonic Day 14 (ED14). The
188 experimental protocol fulfilled the authorization of the "Ministère de l'Enseignement
189 Supérieur et de la Recherche" under the agreement number 01715.01. The Ethics
190 Committee of Strasbourg named "Comité Régional d'Ethique en Matière
191 d'Expérimentation Animale de Strasbourg (CREMEAS)" specifically approved this
192 study. For the innervation experiments, molars were cultured for 6 days on semi-solid
193 medium as previously described [7]. They were then associated with the trigeminal
194 ganglion (TG) on PCL scaffolds (functionalized by PLL/PLGA or PLL/PLGA/CsA) for
195 one night, before subcutaneous implantation for 2 weeks in adult ICR mice.

196 2.6. Histology and indirect immunofluorescence

197 For histology, after 2 weeks implantation, some implants were fixed for 24 h in
198 Bouin-Hollande and embedded in paraffin. Serial sections (7 µm) were stained with
199 Mallory's stain. Sections were observed in a Leica DM4000B microscope. Other
200 implants were embedded in Tissue-Tek, frozen at -20°C and sectioned (10µm) using a
201 cryostat (Leica, CM3000). Serial sections were rinsed with PBS and fixed for 10 min
202 with 4% paraformaldehyde at 4°C. After washing three times for 5 min in PBS at room
203 temperature, sections were incubated for 30 min at room temperature in a blocking
204 solution of 1% bovine serum albumin (BSA) and 0.1% Triton X100 and then incubated
205 for one night at 4°C with the primary antibodies (Table 1). After washing with PBS,
206 sections were incubated with secondary antibodies (Molecular Probes, Invitrogen)
207 (Table 1). Nuclei were stained with 4', 6-diamidino-2-phenylindole (DAPI, Euromedex,
208 Souffelweyersheim, France). Negative controls were performed either omitting the

primary antibody or using normal goat serum (NGS). After 3 additional washes in PBS, slides were mounted in fluorescence mounting medium (Dako, Trappes, France) and observed with a fluorescence microscope (Leica DM4000B).

Table 1. Primary and secondary antibodies used for indirect immunofluorescence

Primary antibodies	**Species origin**	**Manufacturer**	**Dilution**	**Secondary antibodies**	**Dilution**
Anti-Peripherin	Rabbit polyclonal	Abcam	1/600	donkey anti-rabbit Alexa 594	1/500
Anti-CD31	Rat monoclonal	BD Pharmingen	1/200	donkey anti-rat Alexa 488	1/200
Anti-S100β	Rabbit monoclonal	Abcam	1/300	donkey anti-rabbit Alexa 594	1/500
Anti-GAP43	Rabbit monoclonal	Abcam	1/500	donkey anti-rabbit Alexa 594	1/500
Anti-NF200	Rabbit polyclonal	Sigma-Aldrich	1/500	donkey anti-rabbit Alexa 594	1/500
Anti-GFAP	Goat polyclonal	Abcam	1/600	donkey anti-goat Alexa 488	1/200
Anti-Nestin	Goat polyclonal	Tebu-Bio	1/100	donkey anti-goat Alexa 488	1/200

2.7. Scanning and transmission electron microscopies

For the morphological study by scanning electron microscopy (SEM), PCL scaffolds were fixed (4% paraformaldehyde) and dehydrated (successive baths in 25, 50, 75, 90, 100% ethanol) and treated with Hexamethyldisilazane (HDMS). They were stuck on a supporting sample holder using carbon conductive adhesive, then silver-coated and observed with a Philips XL-30 ESEM scanning electron microscope in conventional mode (high vacuum) with a Thornley-Everhart secondary electron detector. For transmission electron microscopy (TEM) observations, samples were fixed by immersion in 2.5% glutaraldehyde and 2.5% paraformaldehyde in cacodylate buffer (0.1 M, pH 7.4), post-fixed in 1% osmium tetroxide in 0.1 M cacodylate buffer for 1 h

at 4°C and dehydrated through graded alcohol series (50, 70, 90, 100%) and propylene oxide for 30 min each under agitation. Samples were embedded in Epon 812. Semi-thin sections were cut at 2 μm with an ultra-microtome (Leica Ultracut UCT), stained with toluidine blue and histologically analyzed by light microscopy. Ultra-thin sections were cut at 70 nm and contrasted with uranyl acetate and lead citrate and examined at 70 kV with a Morgagni 268 D electron microscope. Images were captured digitally by using a Mega View III camera (Soft Imaging System).

2.8. Statistical analysis

The association of cyclosporine with dental development and its association with innervation were evaluated by using the Pearson χ^2 test. The commercial software GraphPad Prism 7.0 for Windows (GraphPad Software Inc.) was used for carrying out the statistical analyses and graphics. Differences between groups were considered significant at $P<0.05$.

3. Results

3.1. Characterization of the nanoparticles and scaffolds

The experimental set up for the continuous synthesis of the CsA-loaded PLGA nanoparticles is depicted in Fig. 1. The synthesis is based on the use of microfluidic platforms (PEEK-based interdigital static micromixer) to achieve a narrow nanoparticle monodispersity with a high throughput and avoiding batch-to-batch product variations. In addition, these nanoparticles were prepared with a portable set-up, where the need for

247 a skilled technician is not required. Those nanoparticles were prepared by an Oil/Water
248 (O/W) microchannel emulsification process and solvent evaporation method.

249 It is important to point out that by using microfluidics no external shear forces
250 are needed compared to the traditional batch production where ultrasonic or mechanical
251 (i.e., homogenizer) forces are needed to form a stable emulsion. Consequently we were
252 able to synthesize CsA-loaded PLGA nanoparticles with just the microfluidic platform.
253 Figure 2 (a-d) shows the morphology of the CsA-loaded PLGA nanoparticles produced
254 in a continuous fashion. Particle sizes of 214 ± 71 nm and 254 ± 63 nm were obtained
255 from the SEM micrograph analysis (N=50) and from DLS (hydrodynamic diameter),
256 respectively. The zeta potentials obtained at physiological pH were -36.33 ±0,21 mV
257 and -28.53 ± 0,41 mV for the PLGA and for the CsA-loaded PLGA nanoparticles,
258 respectively. HPLC analysis revealed an encapsulation efficiency and drug loading of
259 89.6 ± 4.5 % and 9.0 ± 0.4 %, respectively (see definitions in Materials and Methods
260 section).

261 The *in vitro* drug release analysis revealed that after a short induction period a
262 zero order sustained release was achieved and in 14 days a 71% of the encapsulated
263 drug was released from the nanoparticles (see Figure 1 in the Supporting Information
264 section).

265 The PCL scaffolds (Fig. 2e) evidenced a non-woven mesh like structure with a
266 large surface area per volume ratio. Figure 2 (f,g) shows how the CsA-loaded PLGA
267 nanoparticles remained tightly grafted on the surface of the electrospun nanofibers. The
268 layer-by-layer technique was used to decorate the surface of the nanofibers with the
269 PLGA nanoparticles containing the immunosuppressant drug. The preliminary gamma
270 irradiation and ethanol treatment of the electrospun membranes allowed for strong

hydrophilisation of PCL, accompanied by a certain percentage of PCL carbonyl bonds hydrolytic cleavage, leading to the appearance of hydroxyls. This altogether enables the physical adsorption of a first “layer” of cationic polyelectrolyte poly-L-lysine (PLL), allowing further electrostatic attachment of the negatively charged CsA-loaded PLGA nanoparticles.

3.2. Histology of bioengineered teeth implanted for two weeks on $(PLL/PLGA/CsA)_5$ scaffolds

The development of the re-associations seeded on $(PLL/PLGA/CsA)_5$ scaffolds and implanted under the skin of ICR mice for two weeks was evaluated by histological analysis using Mallory’s staining (Fig. 3). Well formed teeth developed: the crown was constituted by several cusps (Fig. 3a) and the formation of root was initiated (Fig. 3a,c,d,h). Blood vessels were observed in all the dental pulp and reached the odontoblastic layer (Fig. 3c,g). Odontoblasts were elongated and polarized, their nucleus was on the opposite site of the secretory pole (Fig. 3c,g). Functional odontoblasts secreted polarized predentin/dentin (Fig. 3b,c,e,g). Dentinal tubules present in the predentin/dentin reached the dentin-enamel junction (Fig. 3e). Elongated ameloblasts were polarized and functional with the synthesis and secretion of the enamel organic matrix (Fig. 3b,e,f). Ameloblasts were in contact with the cells of the stratum intermedium also responsible for the tooth enamel formation (Fig. 3f). Cementoblasts were detected on the surface of the root dentin and secreted the cementum (Fig. 3h).

3.3. Innervation of bioengineered teeth implanted on $(PLL/PLGA)_5$ and

296 $(PLL/PLGA/CsA)_5$ scaffolds in ICR mice

297 Cultured re-associations were co-implanted with trigeminal ganglia for two
298 weeks on PCL scaffolds functionalized with $(PLL/PLGA)_5$ or $(PLL/PLGA/CsA)_5$ under
299 the skin of ICR adult mice. In both these conditions teeth developed with a well formed
300 crown and initiation of the root development as shown by immunostaining experiments
301 (Fig. 4a-d). Antibodies against peripherin were chosen to visualize nerve fibers and
302 against CD31 to detect blood vessels (Fig. 4a-e). In both these conditions re-
303 associations were fully vascularized (Fig. 4a-d). Nerve fibers did not enter the dental
304 pulp after implantation with PCL $(PLL/PLGA)_5$ scaffolds (Fig. 4a,b). Nerve fibers
305 coming from the trigeminal ganglion were detected only in the tissues surrounding the
306 bioengineered teeth at the limit between the dental pulp and the peridental mesenchyme
307 (Fig. 4b). On the other hand, after 2 weeks implantation on CsA-containing PCL
308 scaffolds $(PLL/PLGA/CsA)_5$, nerve fibers were detected in the central part of the dental
309 pulp (Fig. 4c-e) and near the odontoblastic layer (Fig. 4d, white square). Nerve fibers
310 were also positive for NF200 (Fig. 4f,h). Complexes between nerve fibers and immature
311 blood vessels positive for CD31 were formed all over the dental pulp (Fig. 4e,f).

312 Odontoblasts were characterized by immunostaining for nestin (Fig. 4g,h), a
313 marker for differentiated odontoblasts [12,13]. GAP43 is an intracellular growth
314 associated-protein which participates in neuronal and branching during development
315 and regeneration. Staining for GAP43 allowed the visualization of growth cone at the
316 tip of axons (Fig. 4g). Double stainings for GAP43 and nestin showed the presence of
317 GAP43 in the odontoblastic layer (Fig. 4g). The nerve fibers had reached the basal pole
318 of the odondoblasts and were also present between the odontoblasts (Fig. 4g,h). Glial
319 cells were identified using antibodies against S100β for the detection of Schwann cells

and glial fibrillary acidic protein (GFAP) for the detection of satellite glial cells (Fig. 4i). We observed that there are more positive cells for S100β than for GFAP.

Transmission electron microscopy (TEM) showed that in the dental pulp of the bioengineered teeth only unmyelinated axons with low diameter (between 0.5 μm and 1 μm) were present (Fig. 5), while in the trigeminal ganglion there were myelinated and unmyelinated axons. Axons were detected in the dental pulp (Fig. 5a), in the vicinity of blood vessels (Fig. 5b) and near the odontoblasts (Fig. 5c). In axons, microtubules and numerous mitochondriae were observed (Fig. 5). At higher magnification (Fig. 5b'), the diameter of the microtubules could be estimated as 25 nm.

For comparison, seven independent experiments were performed by co-implanting re-associations with trigeminal ganglia on $(PLL/PLGA)_5$ functionalized scaffolds (total number of implants N=19) or on $(PLL/PLGA/CsA)_5$ functionalized scaffolds (total number of implants N=65) during 2 weeks in ICR mice (see the Supporting Information section, Table 1). 66.15% of the $(PLL/PLGA/CsA)_5$ implants regenerated teeth with blood vessels. 88.4% of these formed teeth contained peripheral axons coming from the trigeminal ganglion which colonized the dental pulp up to the odontoblastic layer. 63.15% of $(PLL/PLGA)_5$ implants contained vascularized teeth but nerve fibers stayed in the peridental mesenchyme without going into the dental pulp (see the Supporting Information section, Table 1). Statistical analyses (Figure 6) showed that there was no link between the presence or absence of cyclosporine on the teeth development ($p=0.9117$). On the other hand, the same statistical aanalysis showed that there was a link between cyclosporine and innervation ($p=0.002$).

4. Discussion

The PLGA nanoparticles, widely used in tissue engineering applications, were prepared in a continuous manner by an O/W emulsification process and solvent evaporation method in a microfluidic reactor. It is important to point out that the emulsion was formed without the aid of external mechanical forces (i.e., ultrasonic sources or homogenizers), but only using the shear stress caused by the fluid flow through microfluidic interdigital channels [14]. The polyester PLGA, approved by the FDA in many applications, is biocompatible and biodegradable by hydrolysis of its ester linkages under physiological conditions and excreted from the body as carbon dioxide and water via the Krebs cycle [15,16]. Drug release kinetics of PLGA-encapsulated drugs depend initially on a diffusion-controlled mechanism and at the end of its degradation on an erosion-controlled mechanism. Degradation rates can be tuned depending on the ratio between both monomers, the 50:50 ratio being the one which exhibits the fastest degradation [14]. In this work, the use of this emulsification technique based on microfluidics was effective because the encapsulation efficiency reached was very high 89.6 ± 4.5 % and a drug loading of 9.0 ± 0.4 % was obtained.

The use of these nanoparticles is essential for the functionalization of the PCL scaffolds because the loading levels using the free drug are very low compared to the encapsulation of the drug inside PLGA nanoparticles. Other nanoparticles such as liposomes have been used for the CsA encapsulation to achieve sustained release systems [9,10]. The technique of hot homogenization followed of ultrasonication was used for encapsulation of the cyclosporine [10]. The encapsulation of this drug has been applied in the treatment of infectious digestive diseases, and it was observed that encapsulated CsA showed improved mucosa absorption and reduced side effects [9,10]. CsA encapsulated nanoparticles were also used in dermal applications. Indeed, a

suspension of CsA-loaded nanoparticles has been applied in the treatment of psoriasis, showing an improved outcome [17]. Therefore, the encapsulation of CsA in biodegradable matrices allows a sustained release and reduced unwanted side effects.

PCL scaffolds have already been applied in bone regeneration [18]. The layer-by-layer technique allows controlling the deposition in a sequential manner of drug-eluting nanoparticles on the surface of the PCL fibers. The use of this technique is perfectly adapted to tissue engineering because the molecules incorporated on the scaffold remain active both without degradation and without showing a premature release [19]. In addition, an on-demand release triggered by the presence of cells is achievable by using drug-loaded nanoreservoirs decorating the surface of the scaffold nanofibers. The advantage of this technique is that the amount of active molecules can be controlled through the number of layers on the PCL scaffolds, and consequently the duration of the release. In summary, the use of drug-eluting nanoparticles decorating the surface of scaffolds allows a local action of the active principle with lower doses than the conventional systemic treatment and consequently decreases the risk of toxicity associated to the uncontrolled release of the free molecule.

The development of teeth which formed after two weeks implantation on $(PLL/PLGA/CsA)_5$ scaffolds in ICR mice did not show any differences with those forming after 2 weeks implantation without scaffold [20]. Indeed, the cellular re-associations reached a stage of development equivalent to that of a 4 days postnatal first lower molar (PN4) with a similar crown development and identical mineralization [2,11,20]. To detect axons in the bioengineered teeth, we chose anti-Nf200 and anti-peripherin antibodies. NF200 is expressed in axons from central and peripheral nervous systems. Peripherin is expressed in the nerve fibers from the peripheral nervous system.

Both antibodies detect the axons coming from the trigeminal ganglia innervating teeth *in vivo* [21].

88.4% of the teeth regenerated on $(PLL/PLGA/CsA)_5$ scaffolds contained peripheral axons coming from the trigeminal ganglion which colonized the dental pulp up to the odontoblastic layer. Identical results were obtained in the case of the co-implantation of re-associations cultivated during 7 days with a trigeminal ganglion, implanted during 2 weeks in a ICR mouse treated with CsA [7]. Indeed, in this case, 91.5% of teeth obtained after 2 weeks of implantation in ICR mice treated with CsA in the drinking water were innervated [7]. We can thus conclude that our method of associating a functionalized PCL scaffold with CsA-loaded PLGA nanoparticles is sufficient to obtain innervated teeth and can avoid the side effects related to the ingestion of CsA.

The growth cones positive for GAP43 were present only in the odontoblastic layer in the physiological teeth after birth, forming the mechanic sensory complex [22]. According to Kökten et al. [23] the double staining of the growth cones and odontoblasts did not show the presence of growth cones in the odontoblastic layer in re-associations implanted during 2 weeks in "nude" mice. On the other hand, re-associations co-implanted with a trigeminal ganglion during 2 weeks with CsA-loaded PLGA based scaffolds contained growth cones at the level of the odontoblastic layer. Besides its immunosuppressive action, CsA stimulates the growth of nerve fibers by inducing the expression of the protein GAP43 in the growth cones which could explain the obtained results [24]. In the supporting information section we have included a diagram (see the Supporting Information section, Figure 2) and discussion about the potential mechanisms of action of cyclosporine A on nerve fibrils spouting.

The staining of glial cells with anti-S100ß and anti-GFAP antibodies showed that several populations of glial cells were present in the dental pulp of re-associations implanted with the trigeminal ganglion on functionalized $(PLL/PLGA/CsA)_5$ scaffolds during 2 weeks. The same results were observed for re-associations implanted in "nude" mice, where glial cells were identified in the dental pulp [23]. Several conditions were tested and we observed that these cells were present in the dental pulp in the absence of trigeminal ganglion (data not shown). Thus, these cells did not come from the trigeminal ganglion, as it had been previously suggested [23]. The co-localization between positive GFAP cells and axons coming from the trigeminal ganglion in immunosuppressive conditions suggests cellular communication between these cells. Studies revealed that the positive GFAP and S100ß positive cells secrete numerous cytokines and growth factors such as neurotrophins which favor the axonal survival and regeneration [25,26]. Their origin and their action within the dental pulp remain to be determined.

TEM results showed that the fibers which innervate the teeth dental pulp obtained after 2 weeks of implantation with $(PLL/PLGA/CsA)_5$ scaffolds, were unmyelinated. They also confirmed the relationship between axons and blood vessels because unmyelinated fibers were in contact with endothelial cells surrounding blood vessels. In the physiological conditions, myelinated and unmyelinated axons were observed in the dental pulp of adult rat [27]. It was shown that a nervous lesion leads to a decrease in the number and the diameter of myelinated axons. This decrease in the axon diameter could generate a demyelination [27]. Under our experimental conditions, the dissection of the trigeminal ganglion probably generated this process. Thus, we could suppose that these axons which innervated the dental pulp of the implants were of reduced diameter and consequently deprived of myelin.

5. Conclusions

In conclusion, we developed an implant consisting of an electrospun nanofibrous scaffold functionalized with CsA-loaded PLGA nanoparticles produced by a continuous emulsification process. By using microfluidic reactors it is possible to produce CsA-loaded PLGA nanoparticles with a narrow particle-size distribution and elevated encapsulation efficiency. The layer-by-layer technique allows the deposition of PLGA nanoparticles on electrospun PCL nanofibers in a controlled manner. The proposed system has successfully allowed the innervation of tooth buds. This strategy was validated *in vitro* and *in vivo* and shows its potential application in clinical settings.

Acknowledgments

The authors thank Hervé Gegout for histology and Nadia Messaddeq for the TEM observations. This work was funded by the INSERM. Financial support from the EU thanks to the ERC Consolidator Grant program (ERC-2013-CoG-614715) is gratefully acknowledged. CIBER-BBN is an initiative funded by the VI National R&D&i Plan 2008–2011, Iniciativa Ingenio 2010, Consolider Program, CIBER Actions and financed by the Instituto de Salud Carlos III (Spain) with assistance from the European Regional Development Fund. The corresponding author confirms that all co-authors have reported no conflict of interests. S.K.B., P.S., M.A. and N.B.J. were responsible for project conception and direction. L.P., Y.I.G., A.L., V.S. and A.F. performed experimental work and analyzed the data.

References

[1] B. Dye, G. Thornton-Evans, X. Li, T. Iafolla, Dental caries and tooth loss in adults in the United States, 2011-2012, NCHS Data Brief. (2015) 197.

[2] L. Keller, S. Kuchler-Bopp, H. Lesot, Whole-Tooth Engineering and Cell Sources. In: Huang GT-J, Thesleff I, editors. Stem Cells in Craniofacial Development and Regeneration. John Wiley & Sons, Inc. 2013, pp. 431–446.

[3] M. Siemionow, B. B. Gharb, A. Rampazzo, Pathways of sensory recovery after face transplantation, Plast. Reconstr. Surg. 127 (2011) 1875-1889.

[4] D. Rush, The impact of calcineurin inhibitors on graft survival, Transplant Rev. (Orlando) 27 (2013) 93-95.

[5] A. Roozbehi, M. T. Joghataie, M. Mehdizadeh, A. Mirzaei, H. Delaviz, The effects of cyclosporin-A on functional outcome and axonal regrowth following spinal cord injury in adult rats, Acta Med. Iran. 50 (2012) 226-232.

[6] N. J. Lautermilch, N. C. Spitzer, Regulation of calcineurin by growth cone calcium waves controls neurite extension, J. Neurosci. 20 (2000) 315-325.

[7] T. Kökten, T. Bécavin, L. Keller, J. L. Weickert, S. Kuchler-Bopp, H. Lesot, Immunomodulation stimulates the innervation of engineered tooth organ, Plos One 9 (2014) e86011.

[8] M. Guada, V. Sebastian, S. Irusta, E. Feijoo, C. Dios-Vieitez Mdel, M. J. Blanco-Prieto, Lipid nanoparticules for Cyclospoirne A administration: development, characterization and *in vitro* evaluation of their immunosuppresion activity, Int. J. Nanomedicine 10 (2015) 6541-6553.

[9] M. Guada, H. Lana, A. G. Gil, C. Dios-Vieitez Mdel, M. J. Blanco-Prieto, Cyclosporin A lipid nanoparticules for oral administration: Pharmacodynamics and safety evaluation, Eur. J. Pharm. Biopharm.101 (2016) 112-118.

[10] J. L. Italia, D. K. Bhatt, V. Bhardwaj, K. Tikoo, M. N. V. R. Kumar, PLGA nanoparticles for oral delivery of cyclosporine: Nephrotoxicity and pharmacokinetic studies in comparison to Sandimmune Neoral®, J. Control. Release 3 (2000) 197-206.

[11] S. Eap, T. Bécavin, L. Keller, T. Kökten, F. Fioretti, J. L. Weickert, E. Deveaux, N. Benkirane-Jessel, S. Kuchler-Bopp, Nanofibers implant functionalized by NGF as new strategy to innervate bioengineered tooth, Adv. Healthc. Mater. 3 (2014) 386-391.

[12] C. Terling, A. Rass, T. A. Mitsiadis, K. Fried, U. Lendahl, J. Wroblewski, Expression of the intermediate filament nestin during rodent tooth development, Int. J. Dev. Biol. 39 (1995) 947-956.

[13] A. Quispe-Salcedo, H. Ida-Yonemochi, M. Nakatomi, H. Ohshima, Expression patterns of nestin and dentin sialoprotein during dentinogenesis in mice, Biomed. Res. Tokyo 33 (2012) 119-132.

[14] H. K. Makadia, S. J. Siegel, Poly Lactic-co-Glycolic Acid (PLGA) as biodegradable controlled drug delivery carrier, Polymers 3 (2011) 1377-1397.

[15] D. H. Lewis, Biodegradable polymers as drug delivery systems, Controlled release of bioactive agents from Lactide/Glycolide polymers, in Biodegradable polymers as drug delivery systems. (Ed) M. Chasin, and R. Langer, Marcel Dekker: New York, 1990, pp. 1-43.

[16] M. Chasin, R. S. Langer, Biodegradable polymers as drug delivery systems, Informa Health. M. Dekker: New York, 1990, pp. 347.

[17] G. B. Romero, A. Arntjen, C. M. Keck, R. H. Muller, Amorphous cyclosporin A nanoparticles for enhanced dermal bioavailability. Int. J. Pharmaceut. 498 (2016) 217-224.

[18] C. Mendoza-Palomares, A. Ferrand, S. Facca, F. Fioretti, G. Ladam, S. Kuchler-Bopp, T. Regnier, D. Mainard, N. Benkirane-Jessel, Smart hybrid materials equipped by nanoreservoirs of therapeutics, Acs Nano 6 (2012) 483-490.

[19] E. Leguen, A. Chassepot, G. Decher, P. Schaaf, J. C. Voegel, N. Jessel, Bioactive coatings based on polyelectrolyte multilayer architectures functionalized by embedded proteins, peptides or drugs, Biomol. Eng. 24 (2007) 33-41.

[20] A. Nait Lechguer, M. L. Couble, N. Labert, S. Kuchler-Bopp, L. Keller, H. Magloire, F. Bleicher, H. Lesot, Cell differentiation and matrix organization in engineered teeth, J. Dent. Res. 90 (2011) 583-589.

[21] J. Y. Bae, J. H. Kim, Y.S. Cho, W. Mah, Y.C. Bae, Quantitative analysis of afferents expressing substance P, calcitonin gene-related peptide, isolectin B4, neurofilament 200, and Peripherin in the sensory root of the rat trigeminal ganglion, J. Comp. Neurol. 523 (2015) 126-138.

[22] H. Magloire, M. L. Couble, B. Thivichon-Prince, J. C. Maurin, F. Bleicher, Odontoblast: a mecano-sensory cell. J. Exp. Zool. B Mol. Dev. Evol. 312B (2009) 416-424.

[23] T. Kökten, H. Lesot, S. Kuchler-Bopp, Experimental design for innervation of tooth forming from implanted cell re-associations, In Tech, 2014, ISBN 978-953-51-4114-3

[24] A. Ibarra, E. Hernandez, J. Lomeli, D. Pineda, M. Buenrostro, S. Martinon, E. Garcia, N. Flores, G. Guizar-Sahagun, D. Correa, I. Madrazo, Cyclosporin A enhances

non-functional axonal growing after complete spinal cord transection, Brain Res. 1149 (2007) 200-209.

[25] A. M. Pastor, J. M. Delgado-Garcia, F. J. Martinez-Guijarro, C. Lopez-Garcia, R. R. de la Cruz, Response of abducens internuclear neurons to axotomy in the adult cat, J. Comp. Neurol. 427 (2000) 370-390.

[26] K. Bhatheja, J. Field, Schwann cells: origins and role in axonal maintenance and regeneration, Int. J. Biochem. Cell Biol. 38 (2006) 1995-1999.

[27] X. B. Qian, J. P. Naftel, Effects of neonatal exposure to anti-nerve growth factor on the number and size distribution of trigeminal neurons projecting to the molar dental pulp in rats, Arch. Oral Biol. 41 (1996) 359-367.

Captions

Fig. 1. Experimental set up for the synthesis of PLGA/CsA nanoparticles. PEEK-based interdigital static micromixer (a). Geometry of the inlet stream to assure an equalized flow distribution into the mixing microchannels (b). Detail of the microchannel dimensions (c). Experimental process with the flow rates and stream compositions used and the sequential synthesis, solvent evaporation and polymer precipitation (d).

Fig. 2. SEM (a,b) and TEM (c,d) observation of the resulting CsA-loaded PLGA nanoparticles and SEM visualization of the PCL scaffolds consisting of non-woven electrospun nanofibers (e) grafted with CsA-loaded PLGA nanoparticles after 3 layer-by-layer coatings $(PLL/PLGA/CsA)_3$ (f) or 5 $(PLL/PLGA/CsA)_5$ (g). Bars = 3 μm in a and b, 200 nm in c, 50 nm in d, 1.5 μm in e and 2.5 μm in f and g.

Fig. 3. Histology of bioengineered teeth implanted on the PCL scaffolds functionalized with CsA-loaded PLGA nanoparticles ($(PLL/PLGA/CsA)_5$) for 2 weeks in ICR mice. e and f are magnifications of the selected areas in b which show mineralized matrices and polarized and differentiated ameloblasts respectively. g is a magnification of the selected area in c which shows the polarized and differentiated odontoblasts in contact

560 with blood vessels. h is a magnification of the selected area in d which shows the
561 cementoblasts in contact with the root dentin. Am, ameloblast; BV, blood vessel; Cb,
562 cementoblast; D, dentin; DEJ, dentin-enamel junction; DP, dental pulp; DT, dentinal
563 tubule; E, enamel; Od, odontoblast; pD, predentin; PDL, periodontal ligament; PDM,
564 peridental mesenchyme; SI, stratum intermedium; TG, trigeminal ganglion. Bars = 100
565 μm in a, 25 μm in b-d and 10 μm in e-h.
566
567 Fig. 4. Innervation of bioengineered teeth after implantation based on the PCL scaffolds
568 functionalized with $(PLL/PLGA)_5$ (a,b) and $(PLL/PLGA/CsA)_5$ (c-i). Bioengineered
569 teeth were analyzed immunohistochemically by using selected antibodies as biomarkers
570 for nerve fibers (peripherin, red) and blood vessels (CD31, green) (a-e), which showed
571 that nerve fibers and blood vessels entered the dental pulp after 2 weeks when using
572 PCL $(PLL/PLGA/CsA)_5$ scaffolds (c-e) and that nerve fibers were associated with blood
573 vessels (d and e, white arrowheads). d is a magnification of the dental pulp. On the other
574 hand by using $(PLL/PLGA)_5$ scaffolds only, nerve fibers stayed in the peridental
575 mesenchyme (a,b). Nerve fibers were also stained by NF200 (f,h). They were associated
576 with blood vessels (f, white arrowheads). After 2 weeks of implantation, odontoblasts
577 were stained by an anti-nestin antibody (g,h) and growth cones by an anti-GAP43
578 antibody (g, white arrows). In this case, nerve fibers reached the odontoblast layer (g,h).
579 Immunofluorescence detection of S100β protein and GFAP (i) showed the presence of
580 glial cells as Schwann cells (S100β) and satellite glial cells (GFAP) in the dental pulp.
581 BV, blood vessel; DP, dental pulp; Od, odontoblast; PDM, peridental mesenchyme; TG,
582 trigeminal ganglion. Bars = 200 μm in a and c, 100 μm b and d, 25 μm in e,f and g and
583 10 μm in h and i.

584 Fig. 5. Innervation of bioengineered teeth implanted on the PCL scaffolds
585 functionalized with CsA-loaded PLGA nanoparticles observed by TEM. Unmyelinated
586 axons originating from the trigeminal ganglion and containing numerous mitochondria
587 and microtubules were present in the dental pulp (a) and near the odontoblastic layer
588 (c). An axon was detected near a blood vessel in the dental pulp (b). Note that the
589 diameter of the microtubules was approximately 25 nm (b'). Ax, unmyelinated axon;
590 BV, blood vessel; DP, dental pulp; EC, endothelial cell; m, mitochondria; mt,
591 microtubule; Od, odontoblast; RER, rough endoplasmic reticulum. Bars = 0.5 μm in a,b
592 and c and 0.1 μm in b'.

593 Fig. 6. Effect of CsA-loaded nanofibers on tooth formation and innervation of
594 bioengineered teeth. Values with asterisks are significantly different ** $P<0.01$.

595

596

597

598

599

600

601

602

603

604 TOC

605

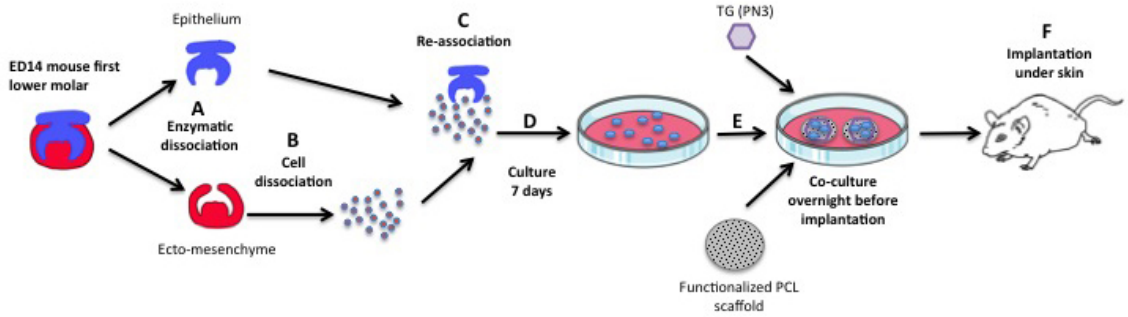

606

607

608

609

Figure 1.

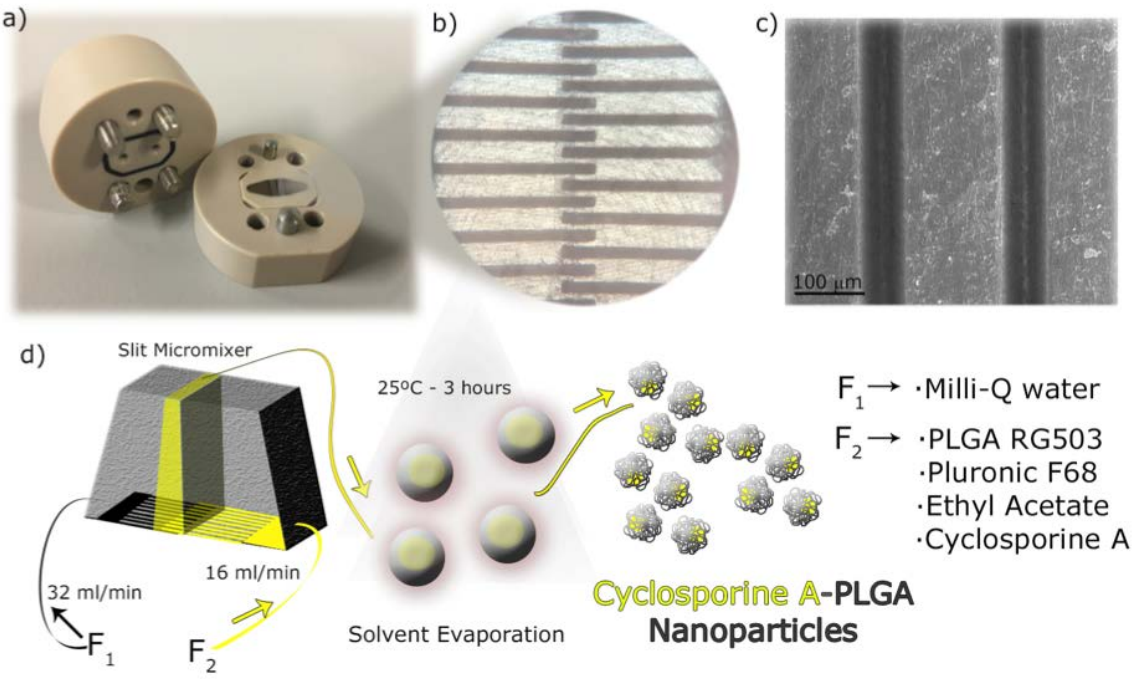
a)
b)
c)
100 µm
d)
Slit Micromixer
25ºC - 3 hours
F1 → ·Milli-Q water
F2 → ·PLGA RG503
·Pluronic F68
·Ethyl Acetate
·Cyclosporine A
16 ml/min
32 ml/min
F1
F2
Solvent Evaporation
Cyclosporine A-PLGA
Nanoparticles

622 Figure 2.

623 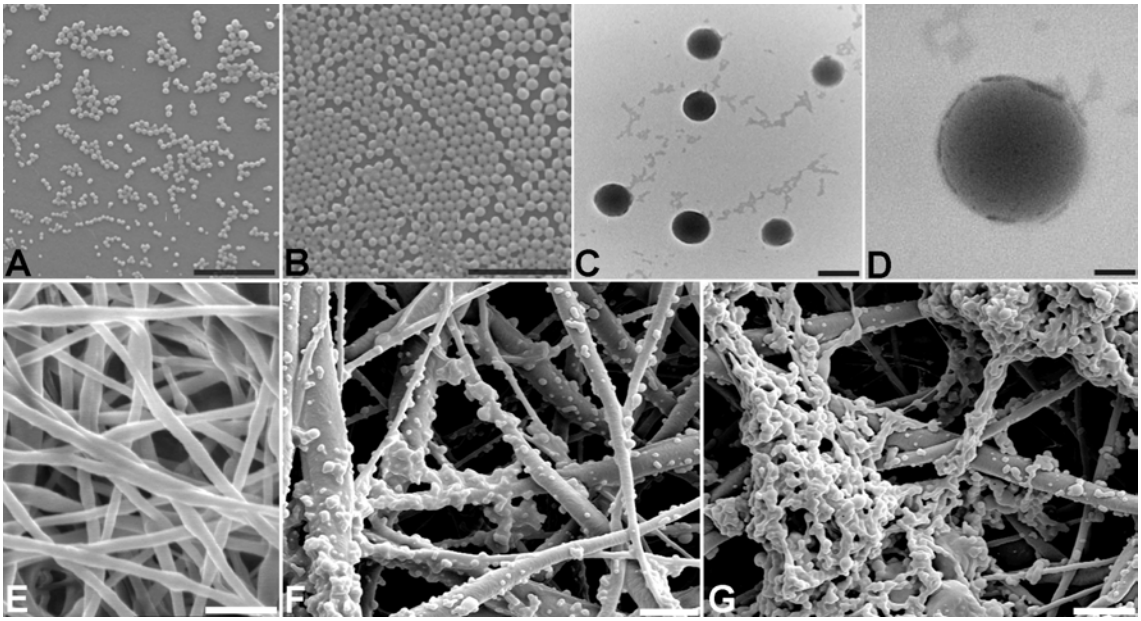

624

625

Figure 3

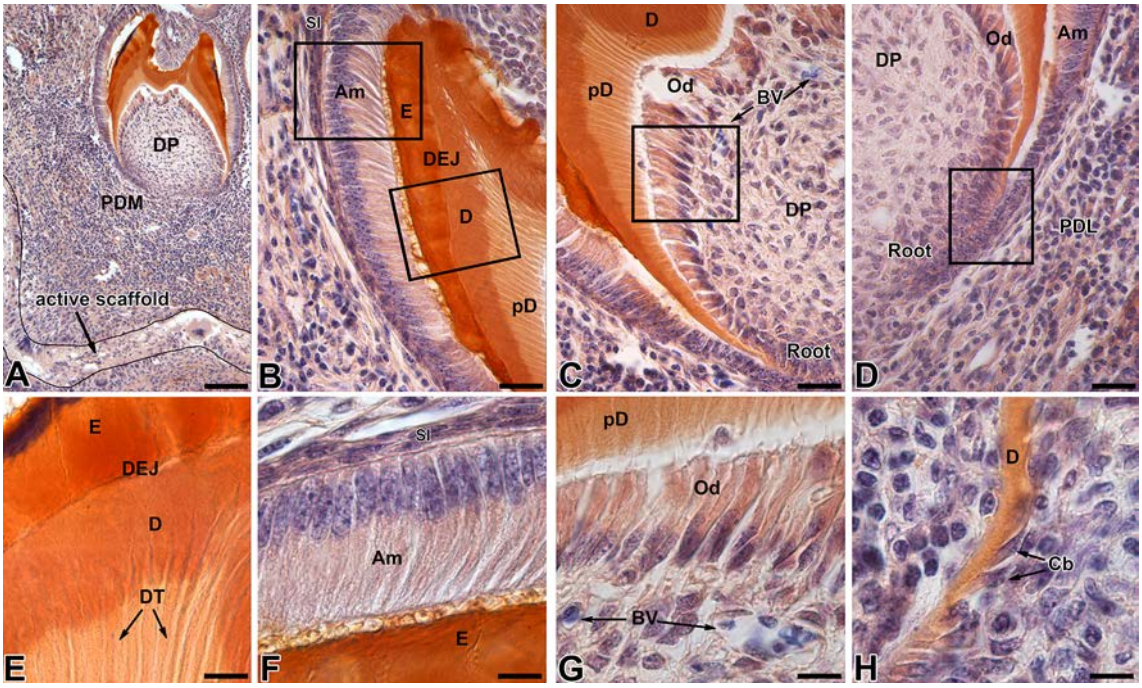
DP
PDM
active scaffold
A
Si
Am
E
DEJ
D
pD
B
D
pD
Od
BV
DP
Root
C
DP
Od
Am
PDL
Root
D
E
DEJ
D
DT
E
Si
Am
E
F
pD
Od
BV
G
D
Cb
H

634 Figure 4

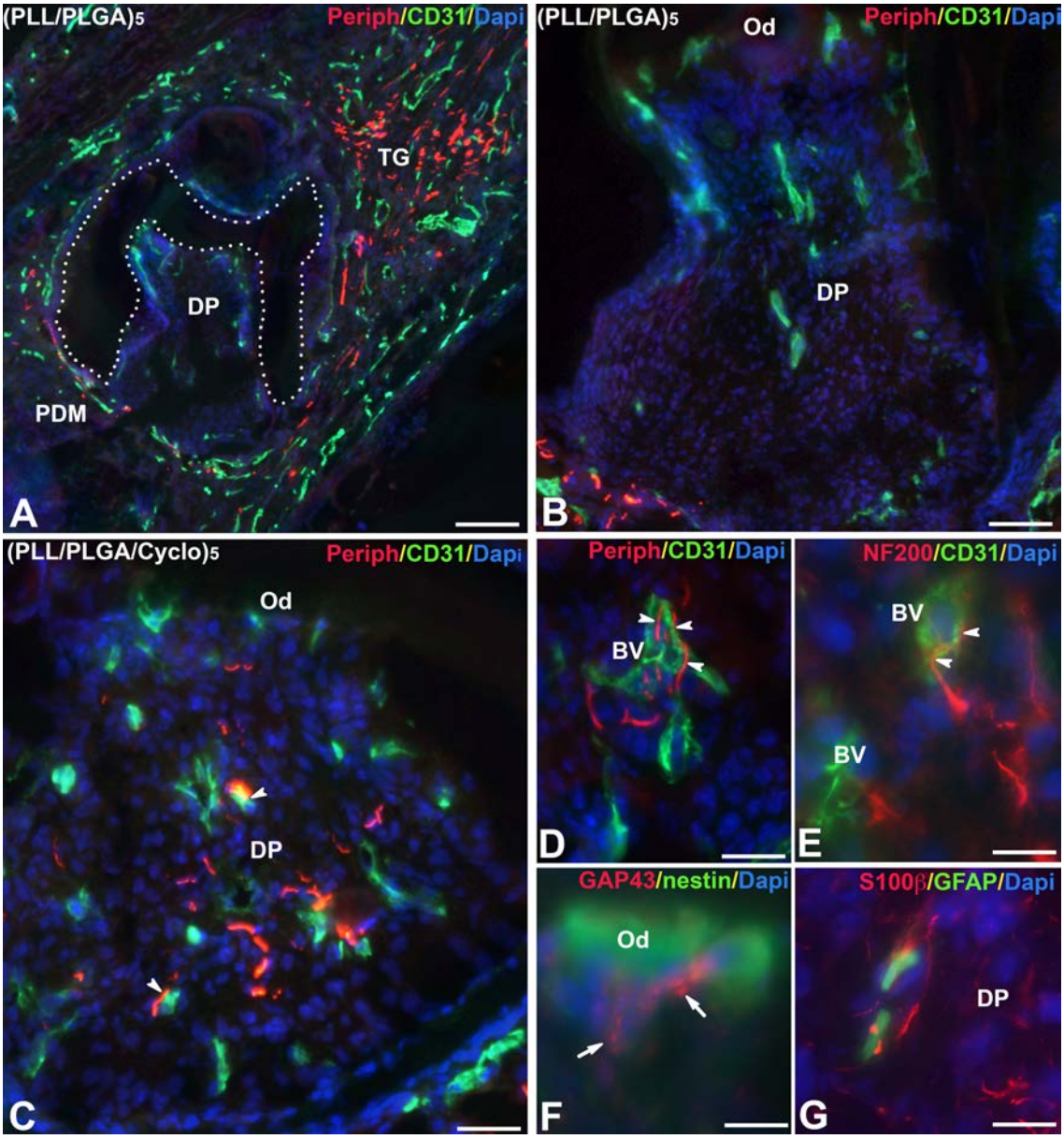

635

636

637

638 Figure 5

639

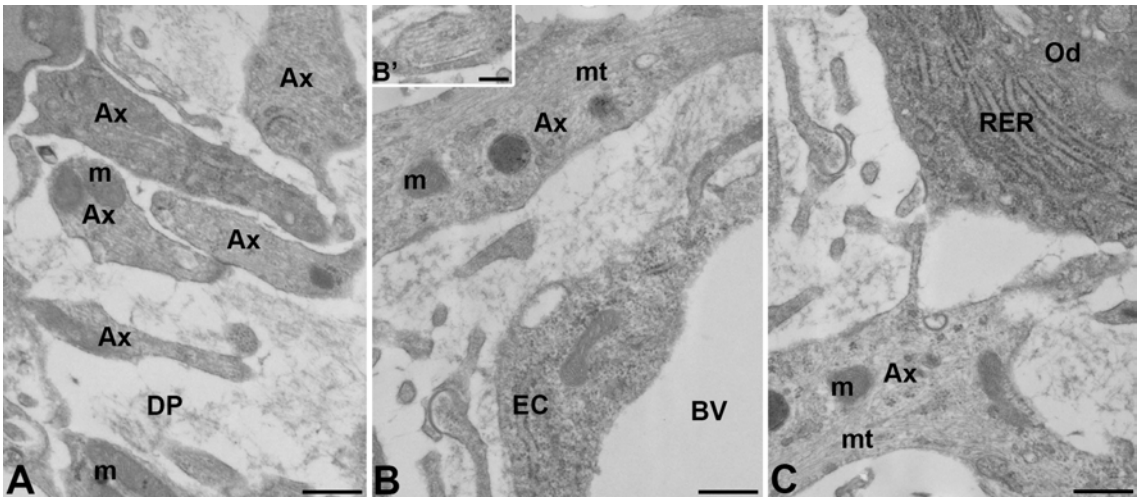

640

641

642

643 Figure 6

644

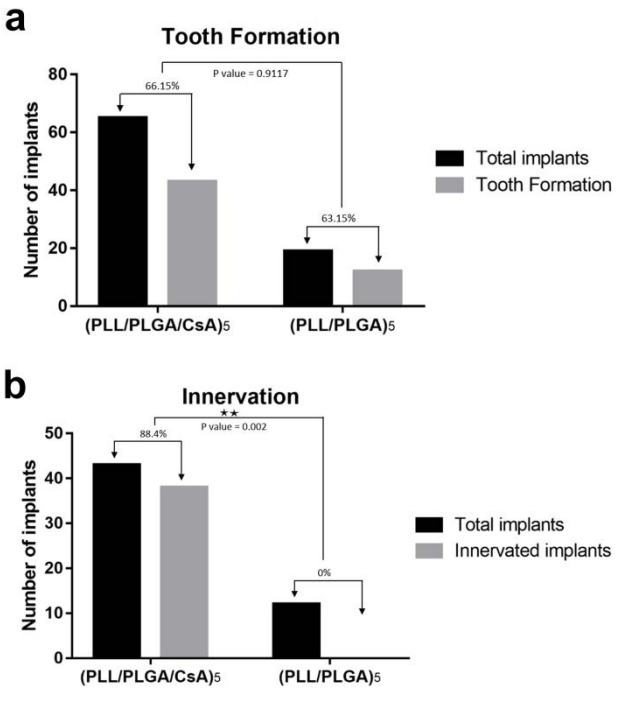

645